Interactions between amino acid side chains in cylindrical hydrophobic nanopores with applications to peptide stability

S. Vaitheeswaran[a] and D. Thirumalai[a,b,1]

[a]Biophysics Program, Institute for Physical Science and Technology, and [b]Department of Chemistry and Biochemistry, University of Maryland, College Park, MD 20742

Edited by Bruce J. Berne, Columbia University, New York, NY, and approved September 24, 2008 (received for review April 24, 2008)

Confinement effects on protein stability are relevant in a number of biological applications ranging from encapsulation in the cylindrical cavity of a chaperonin, translocation through pores, and structure formation in the exit tunnel of the ribosome. Consequently, free energies of interaction between amino acid side chains in restricted spaces can provide insights into factors that control protein stability in nanopores. Using all-atom molecular dynamics simulations, we show that 3 pair interactions between side chains—hydrophobic (Ala–Phe), polar (Ser–Asn) and charged (Lys–Glu)—are substantially altered in hydrophobic, water-filled nanopores, relative to bulk water. When the pore holds water at bulk density, the hydrophobic pair is strongly destabilized and is driven to large separations corresponding to the width and the length of the cylindrical pore. As the water density is reduced, the preference of Ala and Phe to be at the boundary decreases, and the contact pair is preferred. A model that accounts for the volume accessible to Phe and Ala in the solvent-depleted region near the pore boundary explains the simulation results. In the pore, the hydrogen-bonded interactions between Ser and Asn have an enhanced dependence on their relative orientations, as compared with bulk water. When the side chains of Lys and Glu are restrained to be side by side, parallel to each other, then salt bridge formation is promoted in the nanopore. Based on these results, we argue and demonstrate that for a generic amphiphilic sequence, cylindrical confinement is likely to enhance thermodynamic stability relative to the bulk.

confinement effects on protein stability | hydrophobic interactions | potentials of mean force | water in pores

The folding of proteins in confined spaces (1, 2) has received a great deal of attention recently because of its possible relevance to chaperonin-assisted folding (3), the fate of polypeptide chains in the exit tunnel of the ribosome (4), and dynamics in the cellular environment (5, 6). In light of their biological significance, many experimental (1, 7–9) and theoretical studies (10- 16) have examined changes in the confinement-induced stability of proteins. The interplay of several factors, such as alterations in hydrophobic and ionic interactions in confined water, entropic restrictions of the conformations of polypeptide chains, and specific interactions between amino acid residues and the confining boundary determine the stability of proteins (10, 13). Despite the complexity, the observed enhancement in the stability of folded state, compared with that in bulk solvent (1, 7–9), can often be rationalized in terms of the entropic stabilization theory (10–12, 16). However, confinement can also destabilize the folded state (13, 14) because of the alterations in hydrophobic interactions, which can result in a net attraction between the protein and the confining boundary (1, 2).

To provide insights into the experimental studies, we report here interactions between amino acid side chains (SCs) in cylindrical nanopores. A cylindrical geometry is relevant to the conformation of a polypeptide chain in the tunnel of the ribosome (4), the encapsulation of a substrate protein in GroEL (3), and translocation of peptides through biological channels (17). Confinement in a cylindrical pore is expected to greatly alter interactions between SCs because of the interplay of 2 dimensions—L, the length, and D, the cylinder diameter. Quantitative estimates of the free energies of interactions between SCs can provide insights into confinement-induced changes in the stability of polypeptides in such confined geometries. Accordingly, we have calculated the free energies of interaction between the following pairs of side chains: phenylalanine (Phe)–alanine (Ala), serine (Ser)–asparagine (Asn), and lysine (Lys)–glutamate (Glu)—in nanopores. These SCs were chosen as representative examples of large (Phe) and small (Ala) hydrophobic species, polar (Ser and Asn), and charged (Lys and Glu) moieties and are simulated in specific pair geometries.

In a nanopore filled with water at bulk density, the hydrophobic attraction between the side chains of Ala and Phe is destabilized, and the 2 side chains are driven to large separations. At a reduced solvent density $\rho = 0.5\ \rho^{bulk}$, the pair is driven to contact. The orientation dependence of the hydrogen-bonded interactions between the polar side chains of Ser and Asn is greatly enhanced in the nanopore. Confinement also alters the balance between hydrophobic and electrostatic interactions in the Lys–Glu pair. At a particular orientation relative to each other, confinement promotes salt-bridge formation between this pair. Based on our simulations and general theoretical arguments, we predict that confinement in cylindrical pores should enhance the stability of a protein with an amphiphilic sequence. The predictions are explicitly validated by using simulations of 2 tripeptides confined to nanopores.

Results and Discussion

Interactions Between Ala and Phe. We study confinement effects [see *Methods* and supporting information (SI) *Text* for simulation details] in the Ala–Phe pair in 3 relative orientations. In the $\uparrow\bullet$ ($\uparrow\cdot$) orientation, Ala is positioned such that the C_ζ^{Phe}–C^{Ala} (C_γ^{Phe}–C^{Ala}) line is perpendicular to the plane of Phe (Fig. 1). Ala restrained to be in the Phe plane, with the closest Phe atom being C_ζ^{Phe}, is indicated as $\rightarrow\cdot$ (Fig. 2*B*). For reference, we calculated the potential of mean force (PMF) between the 2 SCs in bulk water as a function of r, the distance between their centers of mass (Fig. 1). The PMF for the $\uparrow\bullet$ ($\uparrow\cdot$) pair shows a contact minimum at $r \approx 0.4$ nm and a solvent-separated minimum (SSM) at a separation $r = 0.7$ nm, with an intervening barrier of height $\approx$4.2 kJ/mol (6.2 kJ/mol). The $\rightarrow\cdot$ configuration, in contrast, has

Author contributions: S.V. and D.T. designed research; S.V. performed research; S.V. and D.T. analyzed data; and S.V. and D.T. wrote the paper.

The authors declare no conflict of interest.

This article is a PNAS Direct Submission.

[1]To whom correspondence should be addressed. E-mail: thirum@umd.edu.

This article contains supporting information online at www.pnas.org/cgi/content/full/0803990105/DCSupplemental.

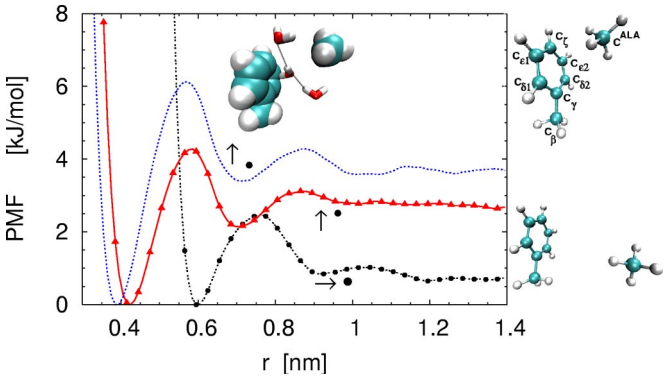

Fig. 1. PMF of unconfined Ala and Phe in bulk water. r is the distance between the centers of mass of the side chains. Curves are translated vertically so that the zero of the scale is at contact. The *Inset* shows the ↑• pair in the SSM. The adjacent stick figures show the geometries of the ↑• (*Upper*), and ↑• (*Lower*) pairs.

a single contact minimum at 0.6 nm with no discernible secondary minimum. The ↑• and ↑• pairs are more stable at contact, relative to large separations, than the →· configuration. Thus, it appears that the preferred orientation of Ala is to have its heavy atom perpendicular to the aromatic ring of Phe in the absence of other steric interactions. Both Phe and Ala are nonpolar, with solvation free energies calculated to be 0.4 and 10.2 kJ/mol, respectively (18), by using the CHARMM22 force field. Therefore, in water-filled nanopores, both solutes will be relegated to the surface (Fig. 3) to maximize the solvent entropy (19).

Fig. 2*A* shows the dramatic effect of confinement on the interaction free energies between Ala and Phe, at different relative orientations, in 2 pores with $D = 1.4$ nm, and $L = 2.2$ and 2.9 nm, with similar results for $D = 2$ nm and $L = 3$ nm (Fig. 2*B*). In the ↑• and ↑• orientations, the SSM at $r = 0.7$ nm is absent in all 3 pores. The barrier between the contact and SSM in the PMF between 2 hydrophobic moieties, such as methane, in bulk solvent, arises because of a single intervening water molecule that is hydrogen-bonded to other water molecules (20). Immediately adjacent to hydrophobic surfaces, such as those bounding the pores, water hydrogen bonds are broken, leading to the instability of the solvent-separated state, and the disappearance of the associated barrier. Therefore, in the nanopore, the SSM and the associated barrier are absent. In bulk water, the barrier has been identified with the free-energetic cost of squeezing out water molecules, thus creating a hydrophobic core in the folding of proteins (21). As noted before (19), the absence of the SSM and the associated barrier in the pores implies that such a model is not applicable in nanoconfinement.

The free energies of the confined ↑• and ↑• pairs show 2 other minima, at separations corresponding to the width and length of the pores. In the pore with $D = 1.4$ nm and $L = 2.9$ nm (Fig. 2*A*), these distant minima are more favorable than the contact minimum by ≈2 and 4 kJ/mol, respectively. In the wider, $D = 2$ nm pore (Fig. 2*B*), the 2 distant minima are equally stable, ≈3 kJ/mol more stable than the contact minimum. When the solutes are restrained to the →· configuration, in addition to the primary contact minimum, there is a single, distant minimum that is less favorable, by ≈4.5 kJ/mol in Fig. 2*A* and ≈3.5 kJ/mol in Fig. 2*B*. The barrier between the 2 minima is substantial, ≈9 − 11 kJ/mol (3.6 − 4.4 k_BT at 298 K) in the narrower pores (Fig. 2*A*), decreasing to ≈7 kJ/mol in the wider pore (Fig. 2*B*).

Free-energy contours in the Phe plane, at a distance of 0.4 nm between the C_γ^{Phe} and the C^{Ala} atoms, in the $D = 1.4$ nm, $L = 2.9$ nm pore, show that this SC pair has a strong tendency (≈6 k_BT) to be oriented with the Ala in a vertical plane relative to the Phe plane (Fig. 4). In such a geometry, the surface areas in

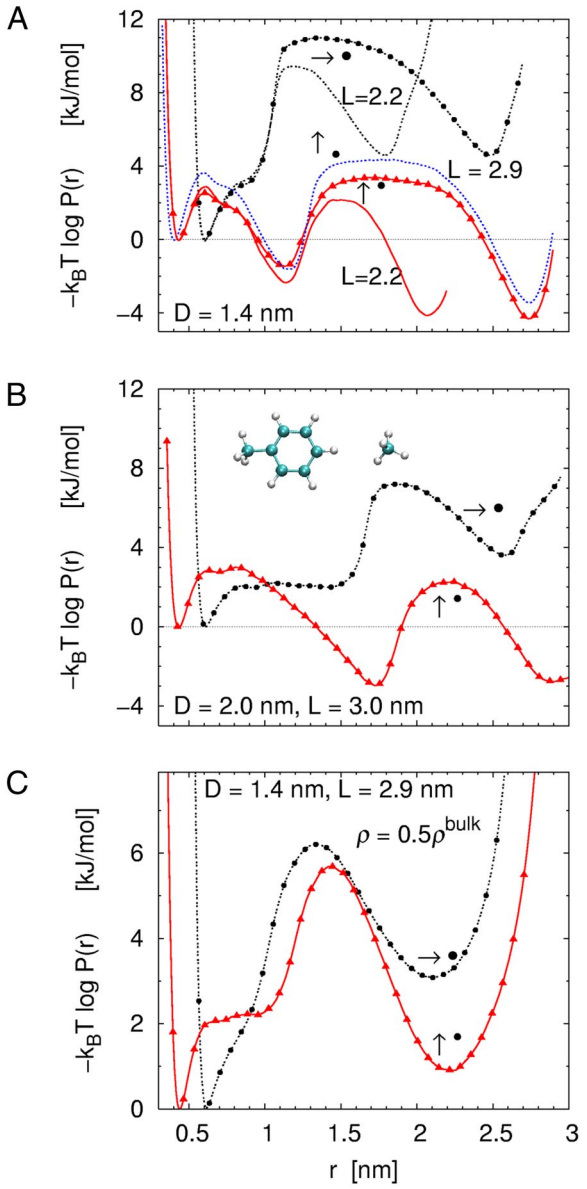

Fig. 2. Free energies of interaction between Ala and Phe. (*A*) Two nanopores, of the same diameter D and different lengths L at bulk water density. In the ↑• and ↑• orientations, confinement destabilizes the contact minimum. (*B*) The $D = 2.0$ nm, $L = 3.0$ nm nanopore at bulk water density. The stick figure shows the →· pair. (*C*) The $D = 1.4$ nm, $L = 3.0$ nm pore with the water density halved.

contact for these 2 SCs are maximized. Because the center of mass of Phe is <0.1 nm from C_γ^{Phe}, both ↑• and ↑• configurations lie in the attractive basin in this figure. A similar orientational preference is also found in bulk water (data not shown).

Interactions Between Hydrophobic Side Chains Are Determined by Accessible Volumes in Solvent-Depleted Zones. The unusual feature of the free-energy profiles when Phe and Ala are confined in the ↑• and →· configurations is the emergence of 2 distinct minima, one at $r \approx D$, the pore diameter, and the other at $r \approx L$, the pore length, that are more stable than the contact minimum. These features of the interaction can be explained by water-mediated ordering as observed near large hydrophobic solutes (22) (see Figs. S1 and S2).

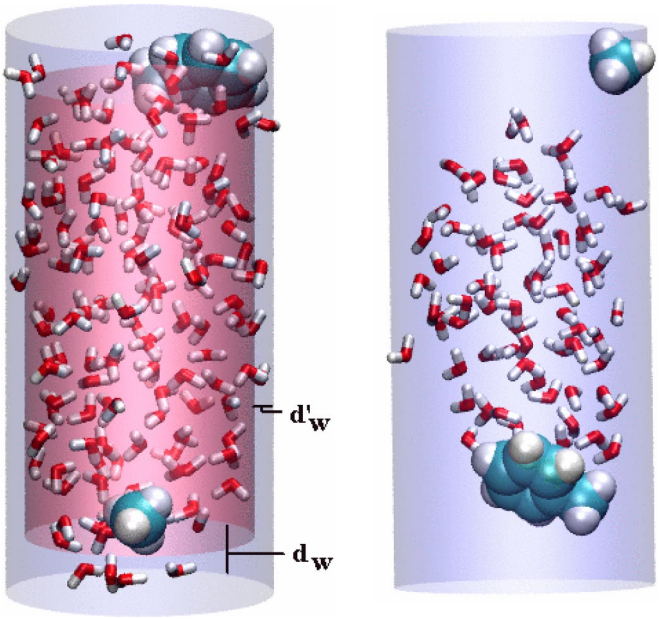

Fig. 3. Snapshots of Phe and Ala in the $\uparrow\bullet$ orientation in the $D = 1.4$ nm, $L = 2.9$ nm nanopore. (*Left*) Water is at bulk density and the SCs are pinned to the hydrophobic walls. Solvent-depleted zones are shown in light blue. The widths of the depletion zones parallel and perpendicular to the cylinder axis are d_w and d_w', respectively. (*Right*) The same system with the water density halved. Here, the SCs are sequestered at the surface of the water droplet.

The results in Fig. 2 can be understood by noting that at the hydrophobic pore boundary, the structure of water is disrupted because of hydrogen-bond breakage. Consequently, there is a zone of depletion of water molecules near the boundary. At equilibrium, Phe and Ala will prefer to be localized at these extended cavities at the water surface (Fig. 3). The planar Phe will be preferentially oriented parallel to the hydrophobic surface, both along the length of the pore and also at the flat end caps, to minimize the hydrophobic area exposed to solvent.

Based on the physical picture described above, we propose a model to explain the free-energy profiles between Phe and Ala. Let us consider the $\uparrow\bullet$ orientation first. If Phe is parallel to the curved surface along the length of the pore, the preference of Ala and Phe for the solvent-depleted region at the surface can be satisfied either when the solutes are in contact or when they

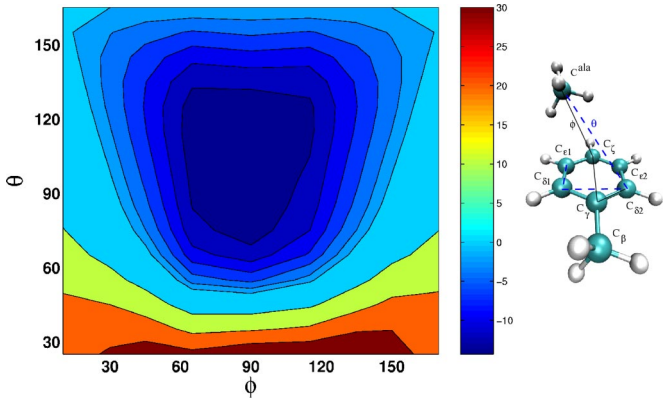

Fig. 4. Free-energy contours (in kJ/mol) as a function of the 2 dihedral angles θ and ϕ in the $D = 1.4$ nm, $L = 2.9$ nm nanopore. The C_γ^{Phe}–C^{Ala} distance is fixed at 0.4 nm. Contours are plotted at 1-k_BT intervals in the region where the interaction free energy is favorable (<0).

are at a separation equal to the pore diameter. Similarly, if Phe is parallel to the flat end caps of the pore, the $\uparrow\bullet$ pair will find thermodynamic equilibrium either at contact or when they are at opposite ends of the pore, at a separation approximately equal to the pore length. At intermediate separations, the network of hydrogen bonds in the cylindrical water droplet will be disrupted, and, hence, these states will be thermodynamically unfavorable. The volume available to the hydrophobic solutes, and hence their entropy, is larger if they are localized at distances $r \approx D$ or $r \approx L$ rather than at the contact distance. Therefore, the contact minimum is metastable in the cylindrical pores. In the $\rightarrow\cdot$ configuration, the solutes can minimize their exposure to solvent only when they are in contact or at opposite ends of the pore. Hence, the free-energy minimum corresponding to the pore width is absent in this configuration. When the $\rightarrow\cdot$ pair is at the opposite ends of the pore ($r \approx L$), Ala is in its preferred environment of low solvent density, but the Phe is constrained to be partially exposed to solvent at bulk density. Consequently, this pair is frustrated between its hydrophobic attraction to the pore surface and the imposed orientational constraints. The distant minimum is therefore metastable relative to the contact minimum.

A simple model that computes the volume available when $r \approx D$ and $r \approx L$ suffices to explain the relative significance of the 2 minima. Let d_w and d_w' be the sizes of the depletion zones near the flat and curved boundary, respectively (Fig. 3). The available volume for the solutes when $r \approx L$ is $V_f \approx 2\ \pi R^2\ d_w$, and $V_c \approx 2\ \pi L\ R\ d_w'$ when $r \approx D$. Here, $R = 0.5D$ is the pore radius. In this model, altering the length of the pore while keeping the width constant will leave V_f unchanged (Fig. 3). This leads to the prediction that the free-energy minimum corresponding to the pore length will have the same stability for pores of different lengths. A comparison of the 2 pores with the same $D = 1.4$ nm and $L = 2.2$ and 2.9 nm in Fig. 2*A*, shows that this is indeed the case for both the $\uparrow\bullet$ and $\rightarrow\cdot$ configurations. The relative depth of the minima [$\propto \ln (V_f/V_c)$] will depend on L, D, d_w, and d_w'. We should emphasize that d_w and d_w' will vary with the wall–water interaction and the extent of drying at the pore surface. Nevertheless, for any pore with hydrophobic walls, there will be a surface region of broken water hydrogen bonds at which nonpolar solutes will prefer to be localized. We therefore expect the interaction free energy of any 2 nonpolar solutes, in a predominantly hydrophobic nanopore, to have distant minima. The relative stabilities of the different states will be sensitive to the force field, particularly the wall–water interaction.

Phe–Ala Interactions Depend Sensitively on Water Density. Water density (ρ) in a confined volume depends critically on the strength of the attraction between the pore wall and water molecules (23, 24). The inert confining boundary in this study does not permit an accurate estimate of the water density inside. Therefore, we arbitrarily reduce the number of water molecules (see *SI Text*) inside the $D = 1.4$ nm, $L = 2.9$ nm pore to $\rho = 0.5\ \rho^{bulk}$. Comparison of Ala–Phe interactions at the reduced ρ in Fig. 2*C*, with the results in Fig. 2*A* shows a striking dependence on the solvent density. Although the net solvent density is low, water molecules in this pore cluster together in a hydrogen-bonded droplet (Fig. 3). The nonpolar solutes are still localized at the surface of the droplet, but the hydrophobic attraction between the solutes and the pore walls is greatly diminished. Interaction free energies for the $\uparrow\bullet$ and $\rightarrow\cdot$ orientations in Fig. 2*C* are similar to each other with 2 minima each—one at contact and the other corresponding to the case where they are located at opposite ends of the droplet. The barrier heights between the 2 minima are similar in both orientations, ≈5.5 − 6 kJ/mol, and the contact minima are favored. Thus, the orientation dependence of the Ala–Phe interaction and the destabilization of the contact pair are strongly modulated by the solvent density. At

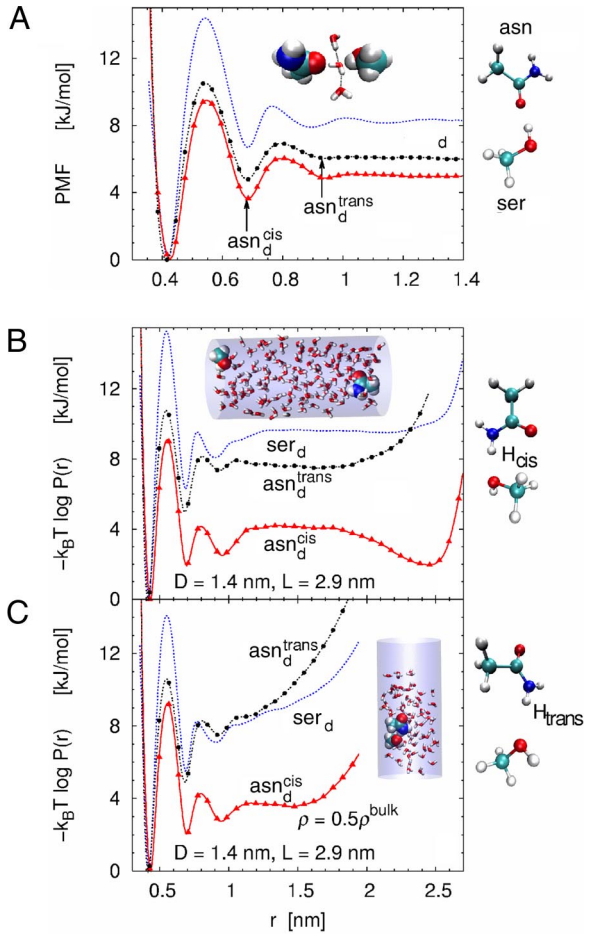

Fig. 5. The 3 configurations of the hydrogen-bonding Ser–Asn pair are shown in the stick figures on the right: (*A*) Ser_d, (*B*) Asn_d^{cis}, and (*C*) Asn_d^{trans}. (*A*) PMF in bulk water. Curves are translated vertically so that the zero of the free-energy scale is at contact. The snapshot shows the Ser_d pair at the SSM. (*B*) Free energies of interaction in a nanopore with $D = 1.4$ nm and $L = 2.9$ nm at bulk water density. The *Inset* shows the system in the minimum at ≈2.5 nm in the Asn_d^{cis} configuration. (*C*) Interaction free energies in the nanopore at half the bulk water density. The *Inset* shows a snapshot of the Asn_d^{trans} configuration.

low ρ, the volumes of the depletion zones are large enough (d_w and d_w' are greater than the size of a water molecule) to accommodate both Phe and Ala close enough to each other ($r \approx 0.6$ nm) to stabilize the contact minimum by favorable van der Waals interactions. At reduced ρ, the hydrophobic attraction between the solutes and the cylinder walls is diminished. The solutes are therefore not strongly pinned to the wall, and the free-energy minimum corresponding to the width of the cylinder is absent in the $\uparrow\bullet$ orientation.

Confinement Alters the Orientation Dependent Ser–Asn Interactions. The 3 hydrogen-bonding configurations of Ser and Asn are shown in Fig. 5 (also see *Methods*). The PMFs between this polar SC pair in bulk water (Fig. 5*A*) show characteristic contact minima (which correspond to the formation of hydrogen bonds) and secondary SSMs. The 2 states are separated by a substantial barrier of 14 kJ/mol for the Ser_d orientation and ≈10.5 and 9.5 kJ/mol for the Asn_d^{trans} and Asn_d^{cis} arrangements, respectively. The Asn_d^{trans} and Asn_d^{cis} pairs have similar energetics in bulk (Fig. 5*A*) but not in cylindrical confinement (Fig. 5*B* and Fig. S3*A*). In bulk water, the contact states in these 2 orientations have similar stabilities relative to large separations of ≈1.4 nm (6 and 5 kJ/mol, respectively). However, in the nanopore, the contact state of the Asn_d^{trans} configuration has much greater stability relative to the same separation (≈7.5 kJ/mol), than the corresponding Asn_d^{cis} case (≈4 kJ/mol). Thus, it is likely that confinement preferentially populates the Asn_d^{trans} geometry in which the *trans* hydrogen (Fig. 5*C*) participates in the hydrogen bond. The confined Asn_d^{cis} pair also shows another, distant minimum at ≈2.5 nm, corresponding to a state in which the solutes are at opposite ends of the pore. The Ser_d pair is only modestly affected by confinement. We also note that the second SSM at ≈0.9 nm becomes more pronounced in the nanopores for all 3 geometries.

The hydrophobic methyl groups of Asn and Ser are expected to be pinned at the pore surface, whereas the amide group of Asn and the hydroxyl group of Ser prefer to be fully hydrated. The conflicting requirements of these chemical groups (methyl, hydroxyl, and amide) can be accommodated in the *trans* geometry at contact, in which both methyl groups can be solvated at the surface and the polar ends remain fully solvated. The favorable surface solvation of both methyl groups, and the direct van der Waals interactions between them, stabilizes the contact state in the *trans* configuration in the pores. In the *cis* configuration, both methyl groups can be located in their preferred environment at the surface only when the 2 molecules are at large distances (Fig. 5*B*). Thus, only at $r > 0.5$ nm can the energetic frustration due to the different preferences of hydrophobic and polar groups be relaxed in nanopores. Comparison of the results in Fig. 5 *A* and *B* show that cylindrical confinement greatly alters the orientation-dependent interactions between Ser and Asn.

Fig. 5*C* shows Ser–Asn interactions in the narrower pore at a lower water density $\rho = 0.5\rho^{bulk}$. Although this is the average water density in the pore, water molecules coalesce into a droplet, leaving empty space in the rest of the pore (Fig. 5*C Inset*). The polar SCs are "bound" to the droplet, and solvent density in the immediate vicinity is close to the bulk. Therefore, in contrast to the hydrophobic Ala–Phe pair (Fig. 2*C*), the polar Ser–Asn pair barely responds to the change in solvent density. The only notable change is the loss of the distant minimum at ≈2.5 nm in the Asn_d^{cis} orientation (Fig. 5*B*).

Balance Between Hydrophobic and Electrostatic Forces Determines Lys–Glu Interactions. The side chains of Lys and Glu carry charges of +e and −e, respectively, at physiological pH. They also have nonpolar parts that prefer to be sequestered from the water. Therefore, the Lys^+–Glu^- pair interaction can be mostly electrostatic or both electrostatic and hydrophobic, depending on their relative orientations. The PMFs between Lys and Glu in the →← and the ↑ ↑ orientations (see *Methods* and Fig. 6) in the bulk show well-defined contact and SSM (Fig. 6*A*). These configurations are stabilized in contact by 8.5 − 10 kJ/mol relative to extended separations. In the nanopores, the →← pair, which is predominantly electrostatic, has the same contact and SSM at ≈0.6 and ≈0.8 nm, respectively, as in bulk solvent (Fig. 6*B*). In this orientation, the free energy has another minimum corresponding to the state where the 2 molecules are approximately a pore length apart, with their charged ends hydrated and the nonpolar ends at the surface. The free energy in the ↑ ↑ orientation shows features of both electrostatic and hydrophobic interactions. This pair is strongly driven to contact at ≈0.43 nm. The shallow SSM at ≈0.8 nm in bulk water is nearly absent in the narrower pore but is discernible in the wider one (Fig. S3*B*).

The Lys–Glu system illustrates how confinement alters the balance between hydrophobic and electrostatic interactions. In the absence of charges, the interaction between these SCs would be entirely hydrophobic. If this were the case, then the free energy of interaction between these hypothetical molecules would have 2 distant minima in addition to the contact minimum, at separations corresponding to the pore dimensions,

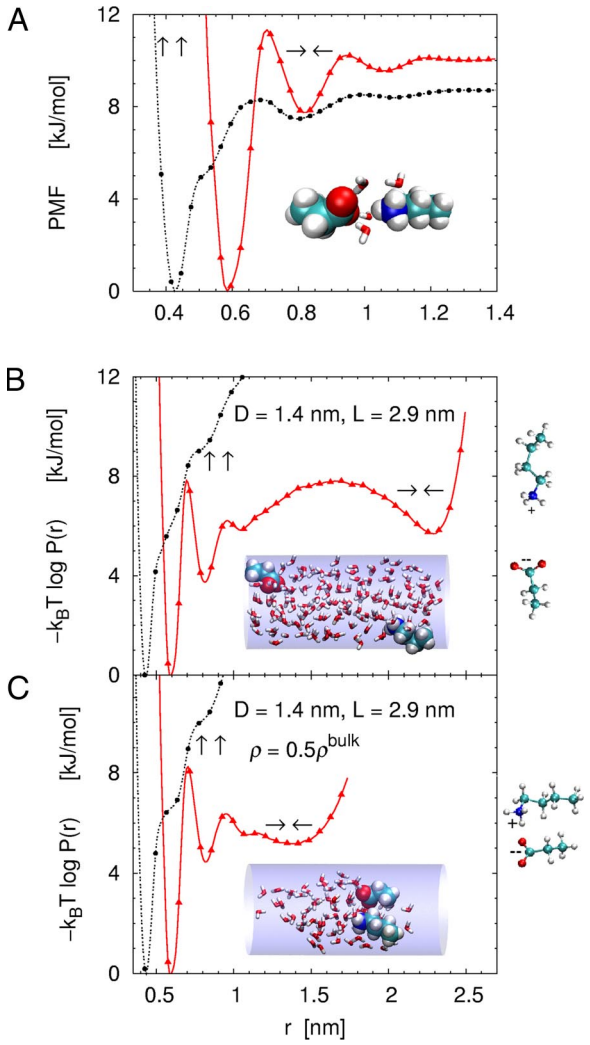

Fig. 6. The polar SCs Lys and Glu are simulated in 2 configurations: →← (stick figure in *B*) and ↑ ↑ (stick figure in *C*). (*A*) PMF between Lys and Glu in bulk water in 2 orientations. Curves are translated vertically so that the zero of the free-energy scale is at contact. The snapshot shows the →← pair at the SSM. (*B*) Free energies of interaction of Lys and Glu in a nanopore of diameter *D* and length *L*. Water is at bulk density. The *Inset* shows the →← pair at the distant minimum at ≈2.3 nm. (*C*) Lys–Glu interaction free energies in the narrower nanopore at half the bulk water density. The *Inset* shows the ↑ ↑ pair at contact.

similar to the Ala–Phe pair. If this was a purely electrostatic pair, the solutes would be fully hydrated and the free-energy profile would have a contact minimum and an SSM but no distant minima. In this scenario, the presence of the confining boundaries will have only a minimal effect on the interaction between the solutes. Because favorable electrostatic interactions are expected to dominate in the bulk, we expect that, in most cases, Lys and Glu will retain their hydration shells. In accord with this observation, it is found that Lys and Glu in Aβ-peptides are solvated in bulk water (25, 26). The orientation-dependent interactions in the nanopore show that confinement (Fig. 6*B*) can promote salt-bridge formation between Lys and Glu.

Just as for the Ser–Asn pair, the Lys–Glu system is largely insensitive to the solvent density (Fig. 6*C Inset*). Fig. 6*C* shows that even with the net solvent density reduced by 50%, both the →← and the ↑ ↑ interactions are similar to those at bulk solvent density (Fig. 6*B*). The distant minimum at ≈2.3 nm for the →← orientation disappears with the decrease in solvent density.

Table 1. Stability changes in peptides confined to cylindrical pores

Pore size (*D*, *L*)*	$\Delta F^{\dagger}$, k_BT	$\Delta F^{\ddagger}$, k_BT
2.0, 2.9	−0.61	−0.84
1.4, 2.9	−0.14 (−0.19)§	−1.50 (−1.02)§

*D and L are the diameter and length of cylindrical pores in nanometers.
†$\Delta F = -\log(P_\alpha/P_\alpha^B)$ for $(Ala)_3$. P_α and P_α^B are the probabilities of being in the α-helical region in the pore and bulk, respectively.
‡ΔF for Lys–Ala–Glu.
§ΔF for $\rho = 0.5\rho^{bulk}$.

Confinement Enhances Peptide Stability. The extent of confinement-induced stabilization (or destabilization) of peptides or proteins, with respect to bulk, will depend on the peptide sequence, entropy loss of the denatured state ensemble (DSE), and solvent density. (*i*) Whereas nonpolar SCs prefer to be localized near the hydrophobic pore boundary, oppositely charged side chains can be stabilized in contact either by the formation of a salt bridge or by interior solvation. Confinement also drives polar SCs to form contacts. (*ii*) Confinement in a narrow cylinder, as is the case in ribosomes, also restricts the rotamer degrees of freedom, thus selecting a particular orientation that may not be preferred in the bulk. The decrease in the rotamer degrees of freedom in nanopores, as well as overall restrictions in the conformations of the peptide, increases the entropy of the DSE. (*iii*) Confinement destabilizes the contact minimum between hydrophobic SCs only if the water density in the nanopore and the bulk are similar. At lower densities, the contact minimum is favored (Fig. 2*C*). These observations suggest that, for a generic polypeptide sequence, confinement should enhance the stability of ordered states.

To test these predictions, we simulated 2 tripeptides, $(Ala)_3$, a hydrophobic sequence, and Lys–Ala–Glu, a hydrophilic sequence with no net charge, in bulk water and in 2 cylindrical pores. Both peptides are in their zwitterionic form, terminated with a positively charged amino group and a negatively charged carboxylic group. In the pores, we find that the center of mass of the $(Ala)_3$ backbone is close to the surface. The charged backbone is hydrated, whereas the nonpolar side chains are sequestered from the water. Not surprisingly, the center of mass of the hydrophilic sequence remains close to the pore axis, away from the surface. These findings are in accord with our expectations based on interactions between amino acid side chains in cylindrical nanopores.

The changes in stability of the peptide conformations, with respect to the bulk, can be assessed by computing the distributions of the backbone dihedral angles ϕ and ψ of the middle residue in each peptide (Fig. S4). The α-helical region is defined as $-80° \le \phi \le -48°$ and $-59° \le \psi \le -27°$ (25). We find that cylindrical confinement stabilizes both peptides, with the hydrophilic sequence being more strongly stabilized (See Table 1). The extent of stability clearly depends on the sequence and its length, pore geometry, and solvent density, just as predicted by using the results for PMFs between amino acid side chains.

Conclusions

The interactions between SCs confined in cylindrical pores are strongly affected by the confining boundary. Hydrophobic solutes, such as Ala and Phe, are driven to the surface to maximize the solvent entropy (19). The solvent density plays a crucial role in determining whether the hydrophobic solute pair is thermodynamically stable in mutual contact or at large separations corresponding to the pore dimensions. The polar side chains in the Ser–Asn pair largely retain their hydration shells and show the characteristic SSM seen in bulk solvent. The Lys–Glu interaction has strong electrostatic as well as hydrophobic com-

ponents and demonstrates the role of confinement on the balance between these forces. Solvent density has only a minimal effect on confinement-induced interactions between both polar and charged SCs.

The explicit calculations for peptides confined to cylindrical pores confirms the prediction that generically, confinement should enhance peptide stability. Nevertheless, if a peptide sequence is strongly hydrophobic, then confinement may destabilize it provided the solvent density in the nanopore is close to the bulk (13, 14, 27, 28). The present results and a number of experiments (1, 7–9) suggest that the decrease in the confinement-induced stability of the folded state, with respect to the bulk, should be an exception rather than the rule.

Materials and Methods

Models. The interaction between the side chains Ala–Phe, Ser—Asn, and Lys–Glu is studied by using molecular dynamics simulations with the CHARMM22 force field (29) and TIP3P water (30). In each amino acid, only the side chain is retained. The carboxyl and amino groups are deleted, and the C_α atom is replaced by a hydrogen atom. Thus, for instance, the side chain of Ala is represented by methane and Phe by toluene.

Solute Geometries. The solutes were maintained in specific orientations relative to each other by using harmonic restraints. For the Ala–Phe pair (see Figs. 1 and 4), these were: (*i*) with the C^{Ala} atom in the same plane as the phenylalanine ring and closest to the C_ξ^{Phe} atom, (*ii*) with the line joining the C_ζ^{Phe} and C^{Ala} atoms being perpendicular to the plane of the phenylalanine molecule, and (*iii*) same as (*ii*) except the C_ζ^{Phe} atom is replaced by C_γ^{Phe}. These 3 orientations are denoted by the symbols $\rightarrow\cdot$, $\uparrow^{\bullet}$, and $\uparrow_{\bullet}$, respectively (the arrow points from C_γ^{Phe} to C_ξ^{Phe}). The 3 hydrogen-bonded orientations of the Ser–Asn pair considered were (*i*) the Ser -OH group as the H-bond donor and the Asn carbonyl oxygen as the acceptor, (*ii*) the Ser oxygen being the H-bond acceptor and the Asn nitrogen and the *trans* hydrogen being the H-bond donor and, (*iii*) same as (*ii*), except that the *trans* hydrogen is replaced by the *cis* hydrogen on the Asn nitrogen. In Asn, we label the hydrogen on the same side of the amide group as the carbonyl oxygen as *cis* and the one on the opposite side as *trans* (Fig. 5). We refer to these as Ser_d, Asn_d^{trans} and Asn_d^{cis}, respectively. For the oppositely charged Lys^+–Glu^- pair, we considered (*i*) the charged ends adjacent to each other and the linear SCs being colinear with each other ($\rightarrow\leftarrow$) and, (*ii*) the charged ends adjacent to each other and the aliphatic parts of the 2 SCs being parallel to each other ($\uparrow\uparrow$). Thus, interactions between the $\rightarrow\leftarrow$ pair are mostly electrostatic, whereas the $\uparrow\uparrow$ pair will have strong electrostatic and hydrophobic interactions.

Simulation Details. In the unconfined systems with bulk solvent, each pair of SCs is solvated in ≈807 water molecules in a cubic cell 3.0 nm in length. The system is equilibrated with periodic boundary conditions at a constant pressure of 1 bar, and a temperature of 298 K. Pressure is maintained by using a Nosé–Hoover Langevin piston, and temperature is controlled via Langevin dynamics. Electrostatic interactions are evaluated by using the particle mesh Ewald (PME) method. PMFs are calculated by using the adaptive biasing force (ABF) technique (31, 32) (see *SI Text* for details) implemented in NAMD (33).

In the pores, interaction free energies, $-k_BT \log P(r)$ [k_B is Boltzmann's constant, r is the distance between the centers of mass of the SC pair, and $P(r)$is the probability of finding the 2 solutes at a separation r], are calculated at a fixed volume by using ABF. Because of the quasi 1-dimensional nature of the confinement when $r \gg D$, we do not subtract the free-energy contribution $-2\,k_BT \log r$, which arises from the increase in phase space proportional to r^2 in spherically symmetric systems. Therefore, these profiles cannot be directly compared with PMFs in bulk. We also calculated free-energy profiles with the C_γ^{Phe}–C^{Ala} distance restrained to a typical contact distance of 0.4 nm to identify the most favorable relative orientation of Ala and Phe at this separation. In this case, the order parameter along which ABF is applied is the dihedral angle $\theta \equiv [C_{\varepsilon 1}^{Phe}\, C_{\delta 1}^{Phe}\, C_{\delta 2}^{Phe}\, C^{Ala}]$ (see Fig. 4). The free-energy profile along θ is evaluated with the dihedral $\phi \equiv [C_{\delta 2}^{Phe}\, C_\gamma^{Phe}\, C_\zeta^{Phe}\, C^{Ala}]$ restrained to fixed values in the range (0°,180°).

ACKNOWLEDGMENTS. Comments on a previous version of the manuscript from Michael Levitt, Bruce J. Berne, Riina Tehver, and anonymous reviewers are greatly appreciated. We are grateful to Michael Levitt for a pertinent remark that led to some of the calculations reported in Fig. 2*A* and Figs. S1 and S2. This work was supported by National Science Foundation Grant CHE 05-14056 and Air Force Office of Scientific Research Grant FA9550-07-1-0098.

1. Eggers DK, Valentine JS (2001) Crowding and hydration effects on protein conformation: A study with sol-gel encapsulated proteins. *J Mol Biol* 314:911–922.
2. Eggers DK, Valentine JS (2001) Molecular confinement influences protein structure and enhances thermal protein stability. *Prot Sci* 10:250–261.
3. Thirumalai D, Lorimer GH (2001) Chaperonin-mediated protein folding. *Annu Rev Biophys Biomol Struct* 30:245–269.
4. Woolhead CA, McCormick PJ, Johnson AE (2004) Nascent membrane and secretory proteins differ in FRET-detected folding far inside the ribosome and in their exposure to ribosomal proteins. *Cell* 116:725–736.
5. Minton AP (2000) Implications of macromolecular crowding for protein assembly. *Curr Opin Struct Biol* 10:34–39.
6. Ellis RJ, Minton AP (2003) Cell biology: Join the crowd. *Nature* 425:27–28.
7. Ravindra R, Zhao A, Gies H, Winter R (2004) Protein encapsulation in mesoporous silicate: The effects of confinement on protein stability, hydration, and volumetric properties. *J Am Chem Soc* 126:12224–12225.
8. Campanini B, *et al.* (2005) Unfolding of green fluorescent protein mut2 in wet nanoporous silica gels. *Prot Sci* 14:1125–1133.
9. Bolis D, Politou AS, Kelly G, Pastore A, Temussi PA (2004). Protein stability in nanocages: A novel approach for influencing protein stability by molecular confinement. *J Mol Biol* 336:203–212.
10. Betancourt MR, Thirumalai D (1999) Exploring the kinetic requirements for enhancement of protein folding rates in the GroEL cavity. *J Mol Biol* 287:627–644.
11. Zhou H-X, Dill KA (2001) Stabilization of proteins in confined spaces. *Biochemistry* 40:11289–11293.
12. Klimov DK, Newfield D, Thirumalai D (2002) Simulations of β-hairpin folding confined to spherical pores using distributed computing. *Proc Natl Acad Sci USA* 99:8019–8024.
13. Cheung MS, Thirumalai D (2006) Nanopore–protein interactions dramatically alter stability and yield of the native state in restricted spaces. *J Mol Biol* 357:632–643.
14. Lucent D, Vishal V, Pande VS (2007) Protein folding under confinement: A role for solvent. *Proc Natl Acad Sci USA* 104:10430–10434.
15. Zhou H-X (2007) Helix formation inside a nanotube: Possible influence of backbone–water hydrogen bonding by the confining surface through modulation of water activity. *J Chem Phys* 127:245101.
16. Ziv G, Haran G, Thirumalai D (2005) Ribosome exit tunnel can entropically stabilize α-helices. *Proc Natl Acad Sci USA* 102:18956–18961.
17. Movileanu L, Schmittschmitt JP, Scholtz JM, Bayley H (2005) Interactions of peptides with a protein pore. *Biophys J* 89:1030–1045.
18. Shirts MR, Pitera JW, Swope WC, Pande VS (2003) Extremely precise free energy calculations of amino acid side chain analogs: Comparison of common molecular mechanics force fields for proteins. *J Chem Phys* 119:5740–5761.
19. Vaitheeswaran S, Thirumalai D (2006) Hydrophobic and ionic interactions in nanosized water droplets. *J Am Chem Soc* 128:13490–13496.
20. Pangali C, Rao M, Berne BJ (1979) A Monte Carlo simulation of the hydrophobic interaction. *J Chem Phys* 71:2975–2981.
21. Cheung MS, Garcia AE, Onuchic JN (2002) Protein folding mediated by solvation: Water expulsion and formation of the hydrophobic core occur after the structural collapse. *Proc Natl Acad Sci USA* 99:685–690.
22. Weiss DR, Raschke TM, Levitt M (2008) How hydrophobic buckminsterfullerene affects surrounding water structure. *J Phys Chem B* 112:2981–2990.
23. Hummer G, Rasaiah JC, Noworyta JP (2001) Water conduction through the hydrophobic channel of a carbon nanotube. *Nature* 414:188–190.
24. Vaitheeswaran S, Yin H, Rasaiah JC, Hummer G (2004) Water clusters in nonpolar cavities. *Proc Natl Acad Sci USA* 101:17002–17005.
25. Klimov DK, Thirumalai D (2003) Dissecting the assembly of $A\beta_{16\text{-}22}$ amyloid peptides into antiparallel β sheets. *Structure (London)* 11:295–307.
26. Tarus B, Straub JE, Thirumalai D (2006) Dynamics of Asp23–Lys28 salt-bridge formation in $A\beta_{10\text{-}35}$ monomers. *J Am Chem Soc* 128:16159–16168.
27. Sorin EJ, Pande VS (2006) Nanotube confinement destabilizes protein helices. *J Am Chem Soc* 128:6316–6317.
28. O'Brien E, Stan G, Thirumalai D, Brooks BR, Factors governing helix formation in peptides confined to carbon nanotubes. *Nano Lett*, in press.
29. Brooks BR, *et al.* (1983) CHARMM: A program for macromolecular energy, minimization, and dynamics calculations. *J Comp Chem* 4:187–217.
30. Jorgensen WL, Chandrasekhar J, Madura JD, Impey RW, Klein ML (1983) Comparison of simple potential functions for simulating liquid water. *J Chem Phys* 79:926–935.
31. Darve E, Pohorille A (2001) Calculating free energies using average force. *J Chem Phys* 115:9169–9183.
32. Henin J, Chipot C (2004) Overcoming free energy barriers using unconstrained molecular dynamics simulations. *J Chem Phys* 121:2904–2914.
33. Phillips JC, *et al.* (2005) Scalable molecular dynamics with NAMD (2005) *J Comp Chem* 26:1781–1802.